Tuning of material properties of ZnO thin films grown by plasma-enhanced atomic layer deposition at room temperature

Julian Pilz, Alberto Perrotta, Paul Christian, Martin Tazreiter, Roland Resel, Günther Leising, Thomas Griesser, and Anna Maria Coclite

Citation: Journal of Vacuum Science & Technology A: Vacuum, Surfaces, and Films **36**, 01A109 (2018);
View online: https://doi.org/10.1116/1.5003334
View Table of Contents: http://avs.scitation.org/toc/jva/36/1
Published by the American Vacuum Society

Tuning of material properties of ZnO thin films grown by plasma-enhanced atomic layer deposition at room temperature

Julian Pilz, Alberto Perrotta, Paul Christian, Martin Tazreiter, Roland Resel, and Günther Leising
Institute of Solid State Physics, NAWI Graz, Graz University of Technology, 8010 Graz, Austria

Thomas Griesser
Institute of Chemistry of Polymeric Materials, University of Leoben, 8700 Leoben, Austria

Anna Maria Coclite[a)]
Institute of Solid State Physics, NAWI Graz, Graz University of Technology, 8010 Graz, Austria

(Received 5 September 2017; accepted 6 November 2017; published 4 December 2017)

The ability to grow inorganic thin films with highly controllable structural and optical properties at low substrate temperature enables the manufacturing of functional devices on thermo-sensitive substrates without the need of material postprocessing. In this study, the authors report on the growth of zinc oxide films by direct plasma-enhanced atomic layer deposition at near room temperature. Diethyl zinc and oxygen plasma were used as the precursor and coreactant, respectively. The process was optimized with respect to the precursor and coreactant dosing as well as to the purging times, which ultimately resulted in saturated atomic layer deposition growth. The so-obtained films exhibit a polycrystalline pattern with a (100) texture and low amount of incorporated carbon. Furthermore, the possibility to tune crystallite size, refractive index, and bandgap of the films by adapting the plasma radio-frequency power is demonstrated. https://doi.org/10.1116/1.5003334

I. INTRODUCTION

Zinc oxide (ZnO) is a wide direct band gap semiconductor ($E_g \sim 3.3$ eV) with attractive optoelectronic and piezoelectric properties.[1] These properties are essential for various applications such as solar cells,[2–4] transparent conductive oxide layers,[5–8] piezoelectric nanogenerators,[9–12] and gas sensors.[13–15] The ability to tune optical and structural properties of the zinc oxide films is crucial for adapting the material characteristics to meet device requirements (i.e., enhanced device efficiency or sensitivity).[16–18] Furthermore, the application of ZnO on thermo-sensitive substrates such as polymers[19–21] and biomaterials[22,23] requires deposition processes operating at low temperatures which should be well below the glass transition temperature of polymers and temperatures that would lead to, e.g., degradation of the biomolecules.

ZnO films can be grown at substrate temperatures around room temperature by techniques such as RF magnetron sputtering,[24] pulsed-laser deposition,[25] and atomic layer deposition (ALD).[1] Tuning of structural and optical properties of the films deposited by these techniques can be achieved by modifying deposition parameters such as RF-power, oxygen pressure, and substrate temperature.

Among other techniques, ALD is the method of choice for the deposition of high-quality conformal layers with Å-level thickness control.[1,26] The growth mechanism is composed of the sequential exposure of the substrate to two (or more) precursors, separated by an inert gas purge. The self-limiting nature of the reactions on the surface offers the possibility for atomic layer precision with a typical growth per cycle (GPC) in the Å/cycle range. The process cycle is repeated until the desired thickness has been achieved. An ALD process in which the surface reactions are driven by thermal energy is called thermal ALD. Typical thermal ALD of ZnO utilizes diethyl zinc (DEZ) and water as the reactants and shows an ALD window (in which the GPC with respect to temperature is fairly constant) of around 110–170 °C.[1]

A variation of ALD that allows lower deposition temperatures to be achieved is plasma-enhanced atomic layer deposition (PE-ALD). In this case, reactive plasma species are used as coreactants.[27] By controlling the plasma process parameters (e.g., pressure, gas composition, and plasma power density), PE-ALD allows material properties to be further tuned. Several groups have been investigating the material properties and growth behavior of ZnO films grown by PE-ALD adopting DEZ as the metal precursor, and oxygen or water-fed plasmas as oxidative coreactants.[1,28–33] A wide range of GPC values has been obtained, spreading from 1.5 to 3 Å/cycle at substrate temperatures of 75–300 °C. The GPC values are clues for different growth mechanisms which cannot be associated with pure ALD growth. It has been reported that the reason behind the variation of the ZnO growth characteristics could be attributed to precursor decomposition effects at substrate temperatures above 60 °C, leading to non-self-limiting growth.[34] Thus, besides the possibility to deposit on thermo-sensitive substrates, depositions which take place below this temperature are highly desired in order to achieve controlled growth and process conditions.

Room temperature deposition of ZnO has been investigated both with thermal and plasma ALD. The growth of

a)Electronic mail: anna.coclite@tugraz.at

zinc oxide at 25 °C by PE-ALD has been reported using dimethyl zinc (DMZ) as the metal precursor, resulting in a GPC of 1.6 Å/cycle.[35] The films are polycrystalline with a preferential (100) orientation and show hydroxyl and bidentate impurities, which are diminished with temperature. Also, thermal ALD of ZnO at 23 °C has been reported using DEZ and water as the metal precursor and coreactant, respectively, resulting in polycrystalline films with a (002) preferential orientation and a GPC of around 0.85 Å/cycle.[36] Films grown at 40 °C show an average carbon content of 1.1 ± 0.3 at. % and a Zn/O ratio of 0.76 ± 0.14 in this study. However, to the authors' knowledge, no previous results have been reported for depositions near room temperature by applying DEZ and O_2-plasma. This low substrate temperature makes it possible to process thermo-sensitive substrates and prevents decomposition effects of the precursor so that controlled ALD-growth can be achieved.

Furthermore, in this contribution, the tuning of ZnO properties has been investigated. In the literature, tuning of structural, optical, and electrical properties has been achieved by modifying process parameters such as substrate temperature,[29,30] O_2-plasma dose,[30] or introducing additional process steps.[37,38] In this study, we investigated the influence of RF-power on the structural and optical properties of the ZnO films and demonstrate a simple approach to tune the crystallite size, refractive index, extinction coefficient, and bandgap for PE-ALD at room temperature.

II. EXPERIMENT

A custom-built direct plasma ALD reactor was used to deposit ZnO thin films on single side polished silicon (100) substrates with a native oxide layer. Prior usage, the substrates were rinsed with isopropyl alcohol and subsequently dried under a CO_2 stream. The reactor was in an asymmetrical plate configuration, in which the showerhead radio frequency (RF) electrode and ground electrode have a clearance of 4 cm and are 20 and 30 cm in diameter, respectively. DEZ (Sigma-Aldrich) was used as the metalorganic precursor. The input power was supplied by an RF-power generator (Advanced Energy Cesar 13.56 MHz) through a matching network (Advanced Energy Navio). The pump system consisted of a turbomolecular pump (Pfeiffer vacuum TMH071P) and a rotary vane pump (Pfeiffer vacuum DUO5M). The pressure in the reactor was controlled via a butterfly valve (MKS 253B). The valve was set to a fixed opening in order to reach a pressure of around 100 mTorr during plasma exposure. A multi gas controller (MKS 647C) and mass flow controllers (MKS MF1-C) were used to control the flow rates of the gases. Pure oxygen was used during the plasma step and Ar was adopted in the purging step. The flow rates for O_2 and Ar were set at 20 sccm during the plasma and the purging step, respectively. An ALD-valve (Swagelok ALD3) was used to pulse DEZ into the reactor. Due to the high vapor pressure of DEZ, no further heating or bubbling system was adopted. One cycle in the ALD process consisted of (1) O_2-plasma dose, (2) Ar purging, (3) DEZ dose, and (4) Ar purging. The process was started with O_2-plasma dose in order to activate the surface. Prior to the plasma exposure, a 10 s O_2 flow stabilization step was introduced to have a constant pressure when igniting the plasma. All depositions were carried out at a floating substrate temperature. The GPC for each deposition was determined by taking the mean value of the layer thickness of two or more samples which were put on different positions in the reactor and dividing it by the number of ALD cycles.

Spectroscopic ellipsometry (J.A. Woollam M-2000V) was used to determine the thickness and optical properties of the films. The measurements were carried out at three different incidence angles (65°, 70°, and 75°) in a wavelength range from 370 to 1000 nm. To determine ZnO layer thicknesses, experimental data were modeled in the ZnO transparent region from 450 to 1000 nm with the COMPLETEEASE software. For this, a three-layer optical model was fitted to the data, consisting of silicon substrate, native silicon oxide layer (fixed thickness of 1.5 nm), and a Cauchy top layer, which accounts for the ZnO. In the Cauchy model, the dispersion relations between the refractive index n and the wavelength λ, as well as between the extinction coefficient k and the energy of the incoming light E, are given by

$$n(\lambda) = A + \frac{B}{\lambda^2} + \frac{C}{\lambda^4}, \tag{1}$$

$$k(E) = k_0 \times e^{D\cdot(E - E_{\text{Bandedge}})}. \tag{2}$$

Here, the variables A, B, C, as well as k_0 and D are fit parameters, while the constant E_{Bandedge} denotes the band edge energy. As parameter C was found highly correlated to parameter B, this parameter was set to 0.

In order to investigate bandgap and near-bandgap absorption, an oscillator model was employed instead of the Cauchy model, fitting the dielectric function over the whole (experimental) spectral range. The oscillator model consists of a Gaussian oscillator to account for high-energy contributions, a PSEMI-M0 model to account for near-bandgap absorption, and another Gaussian oscillator for the near-infrared region.[39] The PSEMI-M0 model is an oscillator with a sharp onset and Kramers–Kronig consistent properties consisting of four connected polynomial spline functions. It is modeled by fit parameters controlling the amplitude, broadening, center energy, left and right endpoints, and left and right midwidth control points.[40] The bandgap energy was obtained by extrapolating the linear part from a $(\alpha h\nu)^2$ vs $h\nu$ plot to intersect the energy axis (Tauc-plot),[41] in which α is the absorption coefficient, h is Planck's constant, and ν is the photon's frequency. The absorption coefficient α was calculated from the measured extinction coefficient k using $\alpha = 4\pi k/\lambda$.[42]

UV-Vis spectroscopy (Shimadzu UV-1800) was used to measure the absorbance of the film deposited on glass in a wavelength range from 190 to 1000 nm and extract the bandgap energy via Tauc fitting. Contributions from reflections were neglected in the analysis.

X-ray diffraction (XRD) in a θ/θ-configuration was performed to analyze the crystalline properties of the films along the specular direction. The diffractometer (Panalytical

Empyrean) utilized radiation of a copper tube monochromatized with a layered x-ray mirror ($\lambda = 1.5418$ Å) and a PIXcel^{3D}-detector which was operated in 1D-mode. A 1/8° divergence slit, a 10 mm mask, and a P7.5 antiscatter slit were used in the setup. Additionally, films were grown on glass substrates and investigated by XRD.

Grazing incidence X-ray diffraction (GIXD) was performed to investigate the in-plane orientation of the crystallites. The measurements were conducted at the Elettra XRD1-beamline in Trieste, Italy. The incident angle α was set between 1.2° and 2° for optimal signal strength and the wavelength λ of the primary beam was either 1 or 1.4 Å. Diffracted intensities were collected on a Pilatus 2M detector and all data have been recalculated to (wavelength-independent) reciprocal space maps utilizing the *xrayutilities* library for PYTHON.[43]

The atomic concentration and oxygen binding state were determined by X-ray photoelectron spectroscopy (XPS) using a Thermo Scientific instrument equipped with a monochromatic Al-Kα x-ray source (1486.6 eV). High-resolution scans were acquired at a pass energy of 50 eV and a step size (resolution) of 0.1 eV. Survey scans were acquired with a pass energy of 200 eV and a step size of 1.0 eV. Photoelectrons were collected using a take-off angle of 90° relative to the sample surface. Charge compensation was performed with an argon flood gun. All analyses were performed at room temperature. For each sample, two different spots were analyzed in pristine conditions and after sputtering with Ar ions. The sputtering was performed at 2000 eV for 5 s. The atom fractions calculated from the XPS survey scans on the two spots were used to calculate average atomic percentages.

III. RESULTS AND DISCUSSION

A. Determination of saturation regimes

In order to ensure self-limited ALD growth and to avoid a chemical vapor deposition (CVD)-like growth mode, each of the four steps in an ALD cycle has to be saturated; that is, the precursor and plasma exposure time should be sufficient to react with all available surface sites, and the purging steps need to effectively remove unreacted precursor molecules, byproducts, and oxidizing species, in order to avoid reactions in the gas phase.[26] In order to minimize the overall processing time, it is desired to operate all four cycles at the minimum time required to obtain saturated growth. The deposition series reported in Table I were performed in order to determine the individual saturation regimes.

TABLE I. Parameters of the deposition series performed in order to determine the saturation regimes.

Series	DEZ dose (s)	Purge after DEZ dose (s)	Plasma dose (s)	Purge after plasma dose (s)
A	**0.31-0.40**	15	15	15
B	0.32	15	**1-40**	15
C	0.32	**2-15**	3	15
D	0.32	5	3	**5-15**

The recipe optimization was performed at RF-power of 100 W for 100 ALD cycles. GPC as a function of the four ALD-cycle parameters is shown in Fig. 1.

The GPC with respect to the DEZ dose saturates at 0.32 s [Fig. 1(a)]. For shorter precursor dosing, the amount of DEZ-molecules is not sufficient to fully react with the available reactive sites.

The GPC with respect to the plasma dose increases with increasing plasma doses and saturates at 3 s [Fig. 1(b)]. Below 3 s, the plasma dose is in an unsaturated regime and thus does not fully remove the organic ligands from the surface reacted DEZ molecules, limiting the growth. On the other hand, plasma doses above 15 s lead to inhomogeneous growth within our setup, which could be due to heating effects of the spatially inhomogeneous plasma leading to different substrate temperatures.

The GPC with respect to the purging after the DEZ exposure decreases when the purging time is increased and saturates at 5 s [Fig. 1(c)]. Below 5 s, the purging time is insufficient to completely remove the unreacted DEZ molecules and reaction by-products, leading to an undesired CVD-like growth of the film. The GPC with respect to the purging after plasma dose also decreases with increasing purging time and saturates at a purging time of 12 s [Fig. 1(d)].

In summary, the optimum recipe in which the GPC saturates for all four partial steps of the ALD cycle with the minimum process time is 0.32 s DEZ dose/5 s Ar purge/3 s O_2-plasma dose/12 s Ar purge. The resulting GPC is ∼1.5 Å/cycle, which is comparable to reported values for the GPC of PE-ALD ZnO films using DEZ and O_2-plasma at the lowest temperatures investigated[28–32] [(∼2.0 Å/cycle at 100 °C,[28] ∼1.7 Å/cycle at 100 °C,[29] ∼2.5 Å/cycle at 100 °C,[30] ∼1.5 Å/cycle at 100 °C,[31] and ∼1.9 Å/cycle at 75 °C (Ref. 32)] and also comparable to the GPC of PE-ALD ZnO using DMZ and O_2-plasma at room temperature (∼1.6 Å/cycle).[35]

With the optimized recipe, films were deposited with 300 ALD cycles and an RF-power of 100 W both on Si and glass substrates and the optical and structural characteristics of the layers were investigated.

The refractive index of the film at 633 nm on the Si substrate obtained by spectroscopic ellipsometry is 1.876 ± 0.003 and 1.877 ± 0.002 using the Cauchy and PSEMI-M0 model, respectively. The results are well comparable with the literature as will be discussed later.

The crystalline properties were analyzed using specular XRD (θ/θ-scan) and GIXD. The specular diffractogram is shown in Fig. 2(a). For the ZnO film deposited on glass, distinct peaks are observed at q_z positions of 2.23, 2.41, and 2.54 Å^{-1}, which match with the (100), (002), and (101) position of a reference ZnO powder. For the ZnO film deposited on Si, the (100) and (101) peak are clearly present, whereas the (002) peak is absent, which could be due to an overlap with the Si (200) peak stemming from the substrate. Both samples show a polycrystalline pattern with a (100) texture (the (100) plane is preferentially aligned parallel to the substrate). Figure 2(b) shows a GIXD-map of the sample deposited on Si which provides additional information about the in-plane orientation of the crystallites. We observe

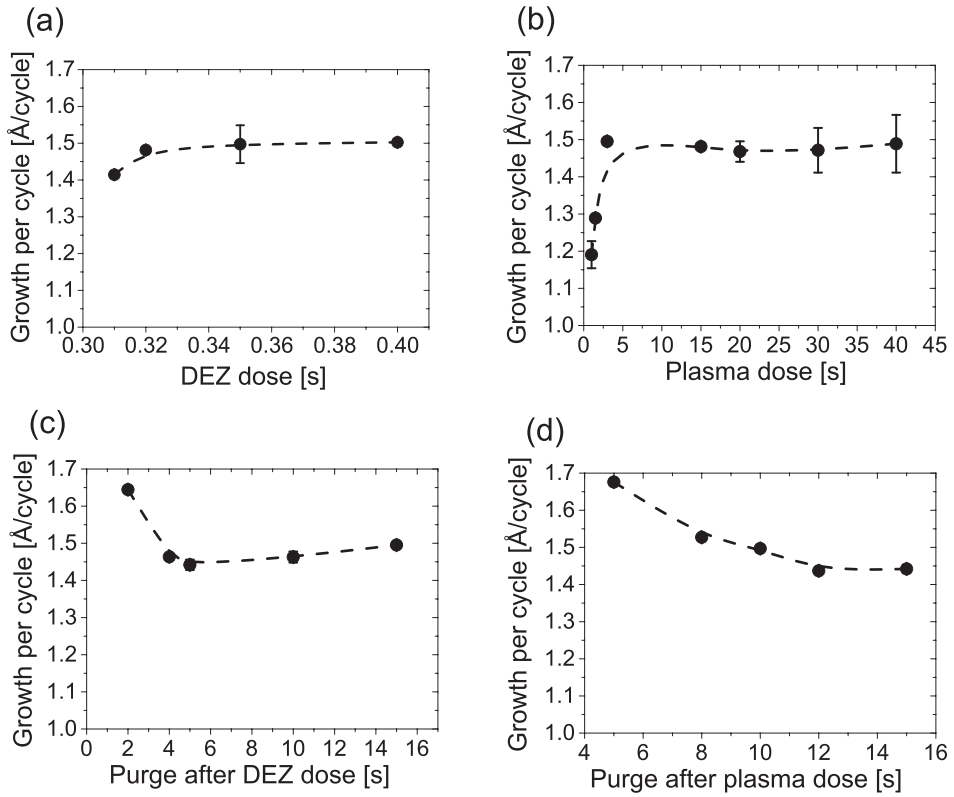

FIG. 1. Growth saturation curves with respect to (a) precursor (DEZ) dose, (b) plasma dose, (c) purging after precursor dose, and (d) purging after plasma dose. Broken lines serve as a guide to the eye. The error bars are plotted for each data point but are within the marker size in most cases.

diffraction rings for the (100), (002), and (101) reflection, which match with the ZnO powder reference. Note that the (002) peak appears preferred in the in-plane direction. This confirms the observation from specular diffraction [Fig. 2(a)] that the ZnO film features a (100) texture.

In the literature, different crystal orientations have been reported for ALD-grown ZnO at different substrate temperatures. From the reported results, it is suggested that, besides temperature being the most influential parameter for the crystal growth,[1] the obtained orientation also depends on the substrate choice and the reaction mechanism (thermal or plasma-enhanced ALD).

In agreement with our results, on Si(100) substrates, polycrystalline ZnO films with a (100) preferential orientation have been obtained by thermal ALD (using DEZ and water),[14] PE-ALD (using DEZ and O_2-plasma),[31] and PE-ALD (using DMZ and O_2-plasma)[35] at 130, 100, and 25 °C, respectively. However, a study of thermal ALD (using DEZ and water) at 23 °C yielded ZnO with a (002) preferential orientation.[36]

On glass substrates, polycrystalline films without preferential orientation have been reported from PE-ALD (using DEZ and O_2-plasma) at 100 °C,[29] while depositions on ITO/glass substrates yielded rather amorphous films.[30]

XPS was used to investigate how the process parameters influence the chemical composition. Two different conditions were investigated. One sample was prepared with the optimized recipe while the other one was prepared with a shorter plasma exposure of 1 s. Both samples were sputtered to remove carbon contaminations from the surface. The results of the compositional analysis as well as the Zn/O-ratios of the pristine and sputtered samples are shown in Table II.

For the pristine samples, the one prepared with the optimized recipe shows less amount of carbon and a higher Zn/O-ratio (24.0 ± 0.3 at. % and 0.76 ± 0.02, respectively) compared to the one prepared with an unsaturated plasma dose (31.7 ± 0.1 at. % and 0.51 ± 0.01, respectively). This could be due to the fact that for the sample prepared with a shorter plasma dose, the plasma step in the recipe is insufficient to fully oxidize the surface and thus remove the organic ligands. The Zn/O-ratio was further calculated taking into account organic contributions to the O1s spectra as suggested by Payne *et al.*[44] This was done by decomposition of the high-resolution spectrum of the C1s peak obtaining normalized oxygen concentrations of the respective functional groups (alcohol/ether, carbonyl, ester, and carbonate). By subtracting the amount of oxygen in organic groups from the oxygen concentration obtained from the survey scan, a corrected Zn/O-ratio can be calculated, which is free of oxygen contributions from adventitous carbon species (labeled as corrected Zn/O-ratio in Table II). The Zn/O-ratio for both samples increases to values closer to unity (i.e., stoichiometric composition), with 0.94 ± 0.02 being observed for the sample prepared with unsaturated plasma dose and 0.92 ± 0.04 for the sample prepared with the optimized recipe. After sputtering, the amount of carbon is reduced to around 3 and 1 at. % for the sample prepared with unsaturated plasma dose and

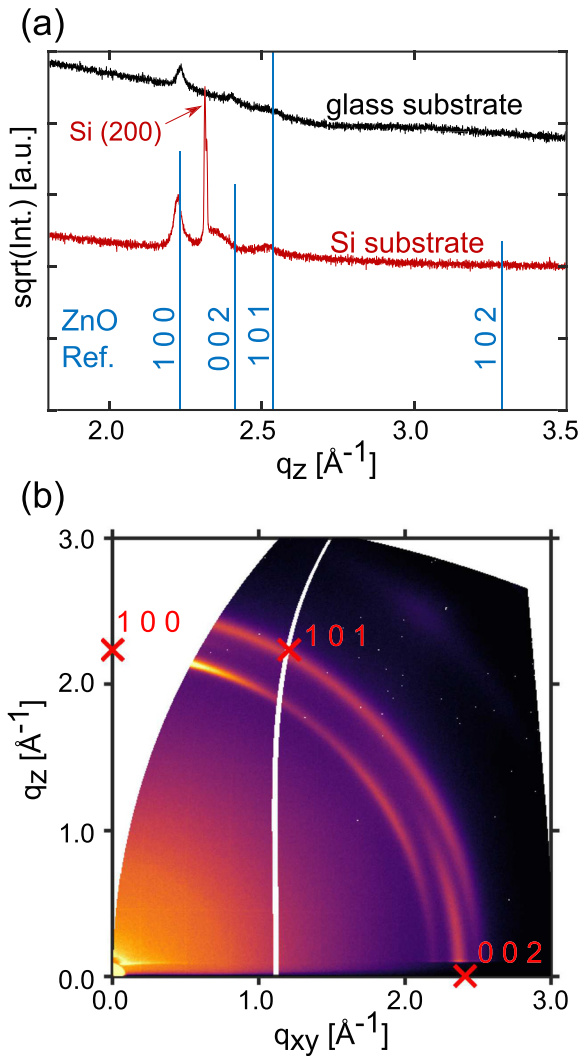

FIG. 2. (Color online) (a) Specular XRD patterns of films deposited on glass and Si-substrates utilizing the optimized recipe. Vertical lines show the peak positions and relative peak intensities of a ZnO powder reference (ICSD-26170). The spectra are shifted along the y-axis for clarity. (b) Corresponding GIXD-map of the sample prepared on the Si-substrate. Theoretical peak positions of crystalline ZnO in a (100) orientation are indicated by (x) markers and labeled with their respective *hkl* values.

optimized recipe, respectively. The Zn/O-ratio increases for both samples to a value slightly larger than 1 which is comparable to literature results.[45] However, preferential sputtering of oxygen could influence this ratio.[46]

High-resolution XPS scans of the O1s spectrum were performed on the two above mentioned samples after sputtering to obtain information about the chemical environment of the oxygen in the film. The results are shown in Fig. 3. The measured peak (dotted) can be decomposed into three peaks at around 530.5, 531.1, and 532.6 eV, which may be attributed to the oxygen-zinc (O-Zn) binding state, oxygen vacancy (Ov), and hydroxyl group (O-H), respectively.[47] Oxygen vacancies reduce the screening of the nearest-neighbor oxygen ions and thus raise the effective nuclear charge which leads to a shift toward higher binding energies (medium peak).[48] It can be seen that the shoulder of the measured peak at around 532.6 eV, corresponding to the OH-groups, is reduced for the sample prepared with the optimized recipe compared to the sample prepared with an unsaturated plasma dose.

B. Tuning of structural and optical properties by RF-power

To investigate the effect of the RF-power on optical and structural properties, films were prepared with 300 cycles of the optimum recipe and varying the RF-power from 30 to 150 W. Figure 4(a) shows the diffractograms around the ZnO (100) peak for samples prepared with different RF-power. It can be seen that both peak position and intensity change with the applied RF-power, pointing out an effect on the *d*-spacing of the crystallites and on the amount of crystalline material being present in the film, respectively. The peak position shifts steadily to smaller q_z-values for higher powers, which means that the *d*-spacing in the (100)-direction is enlarged for higher powers from 2.811 Å for 30 W to 2.825 Å for 150 W. This could be due to defects or microstrain within the films. By increasing the RF-power, the peak intensity increases and saturates for RF-powers in the range 80–120 W and decreases again at 150 W.

In contrast, Kwon *et al.*[38] reported no significant changes in crystallinity and crystal orientation for RF-powers in the range of 50–200 W, but an increase in both resistivity and O/Zn-ratio for increasing RF-power. A possible explanation is the difference in substrate temperature; while their depositions were carried out at 100 °C, the present depositions were carried out near room temperature. Additional influencing factors are different reactor geometries and plasma densities.

An estimation of the average crystallite size *D* in specular direction can be obtained from a Bragg peak in the diffractogram using Scherrer's formula,[49]

TABLE II. Elemental compositions and Zn/O-ratios of ZnO films prepared with an unsaturated plasma dose and with the optimized recipe. Data are stated as mean values of two XPS survey scans on different sample spots and have been determined both for pristine and for surface sputtered samples. The corrected Zn/O-ratios correspond to a ratio corrected with regard to adventitious carbon (see text).

	Oxygen (at. %)	Zinc (at. %)	Carbon (at. %)	Zn/O-ratio	Corrected Zn/O-ratio
Unsaturated plasma dose					
Pristine	45.1 ± 0.1	23.2 ± 0.1	31.7 ± 0.1	0.51 ± 0.01	0.94 ± 0.02
Sputtered	48.0 ± 0.1	49.3 ± 0.4	2.7 ± 0.4	1.03 ± 0.01	
Optimized recipe					
Pristine	43.1 ± 0.2	32.9 ± 0.5	24.0 ± 0.3	0.76 ± 0.02	0.92 ± 0.04
Sputtered	48.0 ± 0.4	51.0 ± 0.1	1.0 ± 0.3	1.06 ± 0.01	

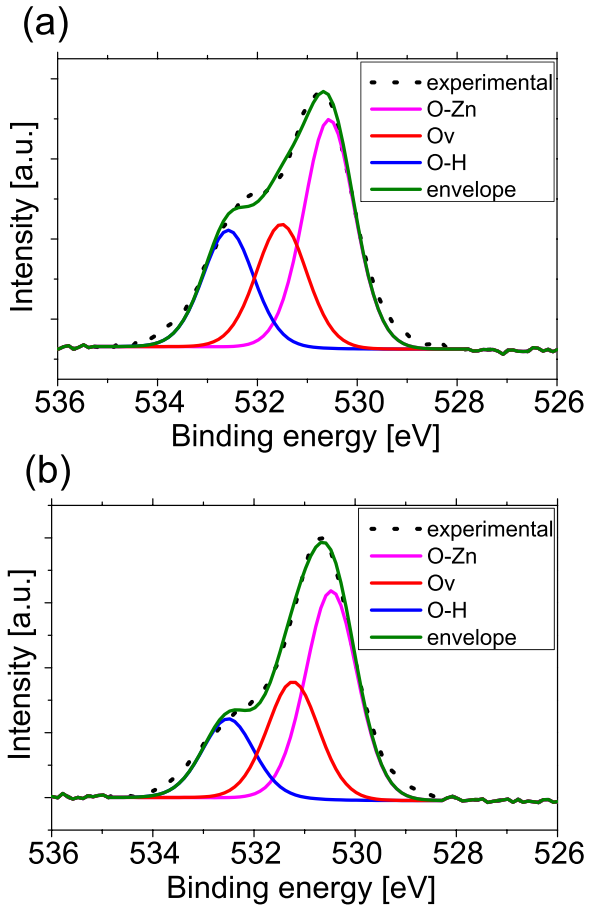

FIG. 3. (Color online) High-resolution O1s peak of (a) a film prepared with an unsaturated plasma dose (1s) and (b) a film prepared with the optimum recipe after sputtering. The experimental peak is decomposed into three Gaussian-peaks which correspond to different binding states of oxygen (see text).

$$D \approx \frac{\lambda}{\beta_{2\theta} \cos\theta}, \tag{3}$$

in which λ is the wavelength of the X-rays, $\beta_{2\theta}$ is the full-width at half maximum of the peak, and θ is the peak position. A plot of the (100) peak position with respect to the RF-power is shown in Fig. S1 in the supplementary material.[56] Figure 4(b) shows the crystallite size with respect to RF-power calculated from the (100) peak properties shown in Fig. 4(a). The crystallite size is about 24 nm for 30 W, rapidly increases to above 26 nm for 40–80 W, and then steadily decreases to 20 nm for 150 W.

These results point out the possibility of tuning the crystalline structure of the films by acting on the RF-power. With this approach, the crystallite size can be tailored to meet specific application requirements, e.g., for photocatalytic applications,[50] where a certain crystallite size of the film is desired.

The growth per cycle and optical properties of the films were measured using spectroscopic ellipsometry. The results for the growth per cycle, refractive index n, extinction coefficient k, and bandgap with respect to the RF-power are shown in Fig. 5.

The growth per cycle [Fig. 5(a)] is constant over the whole range of RF-powers with an average value of ~1.5 Å/cycle.

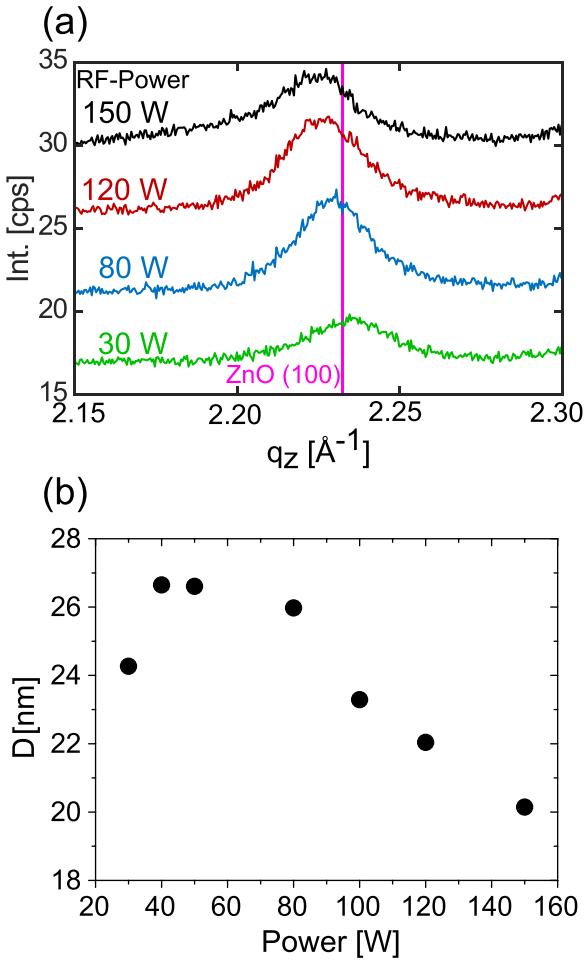

FIG. 4. (Color online) (a) Specular XRD patterns of films prepared at different RF-powers and theoretical ZnO (100) peak position (vertical line). (b) Average crystallite size in specular direction, calculated using Scherrer's formula, as a function of applied RF-power. In (a), the diffraction patterns are shifted in intensity and have been computationally smoothed for clarity.

An increased standard deviation can be seen for samples prepared with 120 and 150 W (also for the refractive index and bandgap) which could be caused by spatial inhomogeneities of the plasma in our setup.

The refractive index n at 633 nm [Fig. 5(b)] is 1.814 ± 0.002 for 30 W, increases rapidly to 1.865 ± 0.003 as power is increased to 40 W and then saturates within the error limits to 1.87 ± 0.01 for RF-powers higher than 50 W. This behavior could either originate from changes in the electronic structure due to variation in defect density or from structural changes of the films (such as the amount of crystalline material, microstrain, or texture as afore-mentioned in the discussion of Fig. 4) introduced by variation of the RF-power. Bond *et al.*[51] obtained a refractive index of 1.99 for a ZnO single crystal at 633 nm, which is 0.12 higher than our obtained value. The refractive index is however well comparable with results obtained for ZnO thin films grown by PE-ALD, magnetron sputtering, and spray pyrolysis,[28,39,52] all of them obtaining refractive index values of ~1.88. (Kawamura *et al.*[28] do not state at which wavelength the refractive index was measured; however, providing a normal dispersion relation, we assume that it has been obtained in the ZnO transparent region.) The

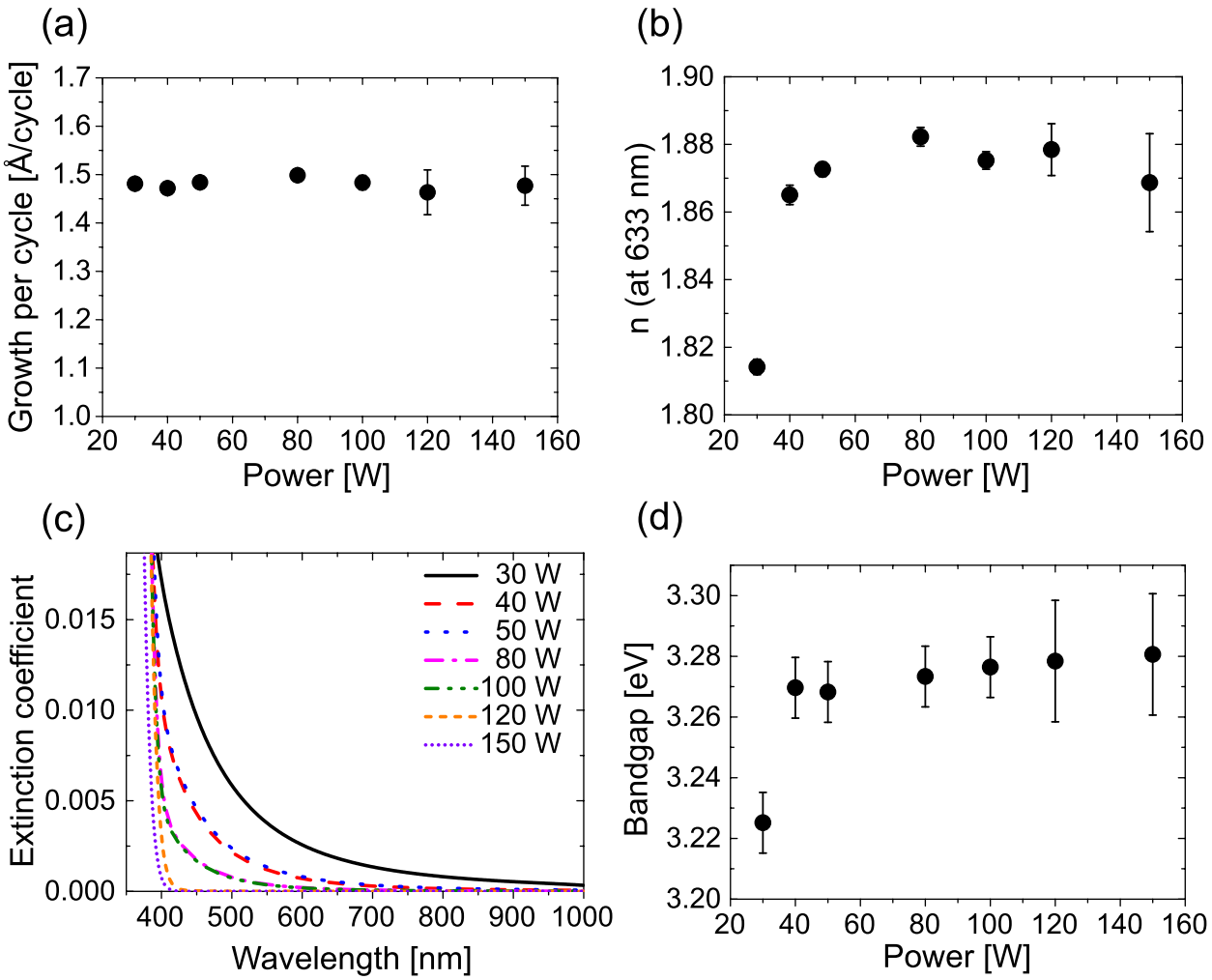

FIG. 5. (Color online) (a) Growth per cycle, (b) refractive index, (c) extinction coefficient spectra, and (d) bandgap with respect to RF-power. The error bars in (a) and (b) originate from the standard deviation of values obtained for films deposited on different positions in the reactor, the spectra in (c) are from samples at the same position in the reactor, and the error bars in (d) originate from the uncertainty in the tangent in the respective Tauc-plots.

tuning of the refractive index together with the precise thickness control of ALD-processes could be used in devices such as dielectric Bragg reflectors.[53]

The spectrum of the extinction coefficient k [Fig. 5(c)] for an RF-power of 30 W shows a smooth transition and k only slowly decays toward higher wavelength, i.e., there is a significant absorption above the bandgap, indicating the existence of defect absorption states (e.g., carbon impurities, O-H groups, or oxygen vacancies, as shown in the XPS analysis).[41] For higher RF-powers, the onset of the absorption becomes sharper pointing out a reduced defect concentration and less absorption at higher wavelengths. For the sample grown with 30 W, the absorption coefficient α is 405.0 and 42.1 cm^{-1} at a wavelength of 633 and 1000 nm, respectively. These values decrease with increasing power and are 26.2 and 1.1 cm^{-1} at a wavelength of 633 and 1000 nm, respectively, for the sample prepared at 100 W.

The bandgap [Fig. 5(d)] shows a rapid increase from 3.23 ± 0.01 to 3.27 ± 0.01 eV when increasing the RF-power from 30 to 40 W and then increases further to 3.28 ± 0.02 eV for 150 W. This allows for bandgap tuning in a small range without the need for dopants,[54,55] applicable in a range of optical and electronic applications. The obtained value for the bandgap using Tauc fitting compares well with the literature; for example, Viezbicke *et al.*[41] found an average value for the bandgap of 3.276 ± 0.033 eV, comparing a large number of publications on thin film ZnO. Furthermore, a sample prepared with 100 W on a glass substrate was analyzed with UV-Vis spectroscopy, the absorbance plot is shown in Fig. S2 in the supplementary material.[56] By utilizing Tauc fitting, a bandgap value of 3.26 ± 0.01 eV was obtained, which is comparable with the value obtained by fitting the spectroscopic ellipsometry spectra.

Concluding, by increasing the RF-power from 30 W to an intermediate range of RF-powers in the range of 40–100 W, the ZnO layers were found to grow with increased refractive index n [at 633 nm, Fig. 5(b)] and with increased crystallite size [for RF-powers in the range 40–80 W, Fig. 4(b)]. The transition of the extinction coefficient was found to become sharper [Fig. 5(c)] and the bandgap shifted toward higher energies [Fig. 5(d)]. We found the RF-power to have no significant influence on the growth per cycle [Fig. 5(a)].

IV. SUMMARY AND CONCLUSIONS

In this contribution, we demonstrate the deposition of polycrystalline ZnO with a (100) texture by PE-ALD at substrate temperatures close to room temperature using DEZ and O_2-plasma as the precursor and coreactant, respectively. Only a few examples are present in literature of studies concerning the combination DEZ, PE-ALD and room temperature deposition, which to the authors' opinion is the most convenient combination in terms of monomer availability (DEZ as opposed to DMZ is largely available), and processing parameters. Especially the access to polycrystalline ZnO at low substrate temperature will enable the exploration of a wide variety of applications for this material, involving polymer hybrids and biomaterials, to name a few.

The ZnO growth within our setup was found to be self-limiting when the length of every ALD cycle was fixed at 0.32 s for the DEZ dose, 5 s for the Ar purge, 3 s for the O_2-plasma dose, and 12 s for the second Ar purge. In these optimized conditions, the GPC was 1.50 ± 0.05 Å/cycle, in agreement with pure ALD growth of ZnO. The refractive index was comparable with ZnO grown by other techniques and the XPS chemical analysis confirmed a Zn/O-ratio close to unity, with a low amount of carbon impurities being present (~1 at. %, after sputtering).

Another interesting aspect is the tunability of optical and structural properties by varying the RF-power. In the range from 30 to 150 W, the crystallite size changed from 20 to 26 nm, the refractive index at 633 nm from 1.81 to 1.88, and the bandgap from 3.22 to 3.27 eV. The possibility to adjust these parameters is extremely important for the use of ZnO deposited by PEALD at near-room temperature for a wide range of devices for optical, electrical, or sensing applications to meet the purpose-specific requirements.

ACKNOWLEDGMENTS

This project has received funding from the European Research Council (ERC) under the European Union's Horizon 2020 research and innovation program (Grant Agreement No. 715403). The authors thank the Elettra-Trieste for the allocation of synchrotron radiation beamtime. The authors are grateful to Nicola Demitri and Luisa Barba for providing assistance in using beamline XRD and Stephan Tumphart and Oliver Werzer for supporting the experiments.

[1]T. Tynell and M. Karppinen, Semicond. Sci. Technol. **29**, 43001 (2014).
[2]M. Law, L. E. Greene, J. C. Johnson, R. Saykally, and P. Yang, Nat. Mater. **4**, 455 (2005).
[3]S. K. Hau, H. L. Yip, N. S. Baek, J. Zou, K. O'Malley, and A. K. Y. Jen, Appl. Phys. Lett. **92**, 253301 (2008).
[4]W. J. E. Beek, M. M. Wienk, and R. A. J. Janssen, Adv. Mater. **16**, 1009 (2004).
[5]X. Jiang, F. L. Wong, M. K. Fung, and S. T. Lee, Appl. Phys. Lett. **83**, 1875 (2003).
[6]K. Ellmer, J. Phys. D: Appl. Phys. **33**, R17 (2000).
[7]H. Kim, C. M. Gilmore, J. S. Horwitz, A. Piqué, H. Murata, G. P. Kushto, R. Schlaf, Z. H. Kafafi, and D. B. Chrisey, Appl. Phys. Lett. **76**, 259 (2000).
[8]M. J. Alam and D. C. Cameron, J. Vac. Sci. Technol., A **19**, 1642 (2001).
[9]Z. L. Wang and J. Song, Science **312**, 242 (2006).
[10]A. Khan, M. Ali Abbasi, M. Hussain, Z. Hussain Ibupoto, J. Wissting, O. Nur, and M. Willander, Appl. Phys. Lett. **101**, 193506 (2012).
[11]G. Zhu, R. Yang, S. Wang, and Z. L. Wang, Nano Lett. **10**, 3151 (2010).
[12]A. Manekkathodi, M.-Y. Lu, C. W. Wang, and L.-J. Chen, Adv. Mater. **22**, 4059 (2010).
[13]C. Wang, L. Yin, L. Zhang, D. Xiang, and R. Gao, Sensors **10**, 2088 (2010).
[14]S.-Y. Pung, K.-L. Choy, X. Hou, and C. Shan, Nanotechnology **19**, 435609 (2008).
[15]S. P. Singh, S. K. Arya, P. Pandey, B. D. Malhotra, S. Saha, K. Sreenivas, and V. Gupta, Appl. Phys. Lett. **91**, 63901 (2007).
[16]Ü. Özgür, Ya. I. Alivov, C. Liu, A. Teke, M. A. Reshchikov, S. Doğan, V. Avrutin, S.-J. Cho, and H. Morkoç, J. Appl. Phys. **98**, 41301 (2005).
[17]H. Xu, X. Liu, D. Cui, M. Li, and M. Jiang, Sens. Actuators, B **114**, 301 (2006).
[18]J. Q. Xu, Q. Y. Pan, Y. A. Shun, and Z. Z. Tian, Sens. Actuators, B **66**, 277 (2000).
[19]M. D. Groner, F. H. Fabreguette, J. W. Elam, and S. M. George, Chem. Mater. **16**, 639 (2004).
[20]S.-H. K. Park, J. Oh, C.-S. Hwang, J.-I. Lee, Y. S. Yang, and H. Y. Chu, Electrochem. Solid-State Lett. **8**, H21 (2005).
[21]E. Langereis, M. Creatore, S. B. S. Heil, M. C. M. Van De Sanden, and W. M. M. Kessels, Appl. Phys. Lett. **89**, 81915 (2006).
[22]M. Knez, A. Kadri, C. Wege, U. Gösele, H. Jeske, and K. Nielsch, Nano Lett. **6**, 1172 (2006).
[23]G. K. Hyde, S. D. McCullen, S. Jeon, S. M. Stewart, H. Jeon, E. G. Loboa, and G. N. Parsons, Biomed. Mater. **4**, 25001 (2009).
[24]E. M. C. Fortunato, P. M. C. Barquinha, A. C. M. B. G. Pimentel, A. M. F. Gonçalves, A. J. S. Marques, R. F. P. Martins, and L. M. N. Pereira, Appl. Phys. Lett. **85**, 2541 (2004).
[25]A. V. Singh, R. M. Mehra, N. Buthrath, A. Wakahara, and A. Yoshida, J. Appl. Phys. **90**, 5661 (2001).
[26]S. M. George, Chem. Rev. **110**, 111 (2010).
[27]H. B. Profijt, S. E. Potts, M. C. M. de Sanden, and W. M. M. Kessels, J. Vac. Sci. Technol., A **29**, 50801 (2011).
[28]Y. Kawamura, N. Hattori, N. Miyatake, M. Horita, and Y. Uraoka, Jpn. J. Appl. Phys. **50**, 04DF05 (2011).
[29]D. Kim, H. Kang, J.-M. Kim, and H. Kim, Appl. Surf. Sci. **257**, 3776 (2011).
[30]M. Jin, J. Jo, G. P. Neupane, J. Kim, K. S. An, and J. W. Yoo, AIP Adv. **3**, 102114 (2013).
[31]J. Zhang, H. Yang, Q. Zhang, S. Dong, and J. K. Luo, Appl. Surf. Sci. **282**, 390 (2013).
[32]S.-H. K. Park, C.-S. Hwang, H.-S. Kwack, J.-H. Lee, and H. Y. Chu, Electrochem. Solid-State Lett. **9**, G299 (2006).
[33]S. M. Sultan, O. D. Clark, T. Ben Masaud, Q. Fang, R. Gunn, M. M. A. Hakim, K. Sun, P. Ashburn, and H. M. H. Chong, Microelectron. Eng. **97**, 162 (2012).
[34]T. Muneshwar, G. Shoute, D. Barlage, and K. Cadien, J. Vac. Sci. Technol., A **34**, 50605 (2016).
[35]P. C. Rowlette, C. G. Allen, O. B. Bromley, A. E. Dubetz, and C. A. Wolden, Chem. Vap. Deposition **15**, 15 (2009).
[36]J. Malm, E. Sahramo, J. Perälä, T. Sajavaara, and M. Karppinen, Thin Solid Films **519**, 5319 (2011).
[37]M. A. Thomas and J. B. Cui, ACS Appl. Mater. Interfaces **4**, 3122 (2012).
[38]J. D. Kwon, J. W. Lee, K. S. Nam, D. H. Kim, Y. Jeong, S. H. Kwon, and J. S. Park, Curr. Appl. Phys. **12**, S134 (2012).
[39]E. Mammadov, N. Naghavi, Z. Jehl, G. Renou, T. Tiwald, N. Mamedov, D. Lincot, and J. F. Guillemoles, Thin Solid Films **571**, 593 (2014).
[40]H. C. M. Knoops, B. W. H. van de Loo, S. Smit, M. V. Ponomarev, J.-W. Weber, K. Sharma, W. M. M. Kessels, and M. Creatore, J. Vac. Sci. Technol., A **33**, 21509 (2015).
[41]B. D. Viezbicke, S. Patel, B. E. Davis, and D. P. Birnie, Phys. Status Solidi **252**, 1700 (2015).
[42]V. Srikant and D. R. Clarke, J. Appl. Phys. **83**, 5447 (1998).
[43]D. Kriegner, E. Wintersberger, and J. Stangl, J. Appl. Crystallogr. **46**, 1162 (2013).
[44]B. P. Payne, M. C. Biesinger, and N. S. McIntyre, J. Electron Spectros. Relat. Phenom. **184**, 29 (2011).
[45]R. Huang, K. Sun, K. S. Kiang, K. A. Morgan, and C. H. De Groot, Microelectron. Eng. **161**, 7 (2016).
[46]E. Guziewicz *et al.*, Semicond. Sci. Technol. **27**, 74011 (2012).
[47]T.-H. Jung, J.-S. Park, D.-H. Kim, Y. Jeong, S.-G. Park, and J.-D. Kwon, J. Vac. Sci. Technol., A **31**, 01A124 (2013).

[48]J. C. C. Fan and J. B. Goodenough, J. Appl. Phys. **48**, 3524 (1977).
[49]M. Birkholz, *Thin Film Analysis by X-Ray Scattering* (Wiley-VCH, Weinheim, 2006).
[50]B. Pal and M. Sharon, Mater. Chem. Phys. **76**, 82 (2002).
[51]W. L. Bond, J. Appl. Phys. **36**, 1674 (1965).
[52]F. Paraguay D., W. Estrada L., D. R. Acosta N., E. Andrade, and M. Miki-Yoshida, Thin Solid Films **350**, 192 (1999).
[53]Z. Yan *et al*., Appl. Phys. Lett. **90**, 143503 (2007).
[54]S. C. Das, R. J. Green, J. Podder, T. Z. Regier, G. S. Chang, and A. Moewes, J. Phys. Chem. C **117**, 12745 (2013).
[55]S. V. Bhat and F. L. Deepak, Solid State Commun. **135**, 345 (2005).
[56]See supplementary material at https://doi.org/10.1116/1.5003334 for the (100) Bragg peak position with respect to RF-power and the absorbance spectrum of a sample prepared with the optimized recipe at 100 W.